Int. J. Heat Mass Transfer. Vol. 17. pp. 899–907. Pergamon Press 1974. Printed in Great Britain

EFFECTS OF SURFACE RESISTANCES ON SIMULTANEOUS HEAT AND MASS TRANSFER IN POROUS SOLIDS WITH PHASE CHANGE

SACHIO SUGIYAMA, MASANOBU HASATANI, MASAAKI NAKAMURA
Department of Chemical Engineering, Nagoya University, Nagoya, Japan

TADASHI MORISHITA
Daicel Co. Ltd., Amagasaki, Japan

and

AKIHIRO KIYOTANI
Sumitomo Light Metal Industry Co. Ltd., Nagoya, Japan

(*Received* 14 *December* 1973)

Abstract—The drying mechanism and the drying rate of porous solids in the usual hot air dryers have been widely analized, and also have been theoretically systematized. However, when the wet solids were dried in a fluidized bed making use of the fact that the heat-transfer coefficients between fluidized bed and solids were remarkably large, such unusual phenomena were found that the inner temperature dropped while drying. Such unusuality has never been expected from conventional theories of hot air dryer.

In this report, the authors dried various solid spheres containing liquids in a fluidized bed, and tried to analize such unusual phenomena with application of the analytical method of drying rate previously presented by us.

NOMENCLATURE

a_i, effective specific area for internal evaporation [m^2/m^3];
a_s, effective area fraction for surface evaporation [m^2/m^2];
C, specific heat [kcal/kg °C];
D_v, vapor-transfer coefficient inside a solid [m^2/h];
D_w, water-transfer coefficient inside a solid [m^2/h];
H, absolute humidity [$kg-H_2O/kg-$dry air];
h, heat-transfer coefficient [kcal/m^2 h °C];
h_{evap}, rate constant of local evaporation [m/h];
k_H, mass-transfer coefficient based on humidity difference [kg/m^2 h ΔH];
k_v, mass-transfer coefficient based on vapor concentration difference [m/h];
L, latent heat of evaporation [kcal/kg];
P, total pressure [atm];
p, vapor pressure [atm];
R, radius of a sphere [m];
R_{loc}, rate of local evaporation [kg/m^3 h];
R_{sf}, constant rate of surface evaporation [kg/m^2 h];
r, distance from the center of a sphere [m];
t, time [h];
u, velocity [m/h];
v, vapor content [kg/kg − dry solid];
W, weight of contained water [kg];
W_s, weight of a dry solid [kg];
W_p, weight of particles caught on the solid surface [kg];
w, water content [kg/kg − dry solid].

Greek letters

ε, porosity;
η, tortuosity factor;
θ, temperature [°C];
λ, thermal conductivity [kcal/m h °C];
ρ, density [kg/m^3].

Subscripts

0, initial values;
I, first stable stage;
II, second stable stage;
a, atmosphere;
C, convection;
c, center of a sphere;

e, wetted state;
F, fluidized bed;
m, midpoint of the surface and center of a sphere;
o, dry state;
s, surface of a sphere;
*, saturated.

INTRODUCTION

It is well known that heat- and mass-transfer coefficients on surroundings of a fluidized bed and on a solid surface fixed in a fluidized bed take very large apparent values [4, 6] by vigorous mixing action of fluidizing gas and particles.

Recently the dryers utilizing fluidized bed have become popular. These fluidized bed drying methods are mainly classified into two kinds: one is to dry wet solid granules which are the fluidizing particles, and the other, to dry large wet solids which are placed inside the bed in which other particles are being fluidized. Shirai *et al.* [4] applied the latter method to perform the drying experiments with the insulating brick sphere (B1 type) as a specimen. They calculated both heat- and mass-transfer coefficients from the experimental results, and discussed the effects of fluidizing particles and gas stream in the fluidized bed on both coefficients.

In this paper, the B1 type brick—which was used by Shirai *et al.* [4]—the B6 type brick and other porous solids which have different pore diameters were dried in the hot air flow (convective drying) and inside a fluidized bed (fluidized bed drying). As for the contained liquids, water, *i*-butyl alcohol and glycerine solution were used. Thus, as varying heat- and mass-transfer resistances on solid surface widely, the characteristics of the temperature change inside the solids and of the drying rate were examined in process of drying. As the results, in case of B1 type brick in which pore diameter is smaller, the temperature changes in the fluidized bed drying were found similar to ones in the convective drying; on the contrary, as for the specimen with comparatively large pore diameter such as B6 type brick, in fluidized bed drying, the unusual temperature changes that were never seen in the convective drying were observed. From the viewpoint that this phenomenon should be analized in the connection of heat and mass transfer rates on solid surface with the rates inside porous solid, the authors have checked the experimental results with application of the analytical method [1] for the drying rate presented previously by the authors.

EQUIPMENT AND PROCEDURES

Specimen

As for porous solids, B1 type and B6 type insulating bricks and many kinds of sintered clay† of various pore diameters were used. And on the basis of the experimental results, finally B1 type brick was regarded as the typical solid of comparatively small pore diameter and B6 type brick as the typical one of larger pore diameter. The characteristic values of these solids are summarized in Table 1, in which the tortuosity factor η is calculated by the method of Shimizu *et al.* [3].

Table 1. Characteristic properties

	B1 brick	B6 brick
ρ_o [kg/m^3]	$0{\cdot}66 \times 10^3$	$0{\cdot}73 \times 10^3$
ε_o	0·593	0·620
λ_e [kcal/m h °C]*	$0{\cdot}170 + 0{\cdot}55w$	$0{\cdot}271 + 0{\cdot}51w$
BET specific surface area [m^2/g] (CO_2 adsorption)	2·54	0·01
η^2 (at $w = 0$)	2·56	1·44

*Measured in a vessel saturated with vapor by unsteady hot wire method.

Pore size distribution curves of B1 and B6 bricks with Hg dilatometer, respectively, reached a peak at approximately 3×10^3 Å and 7×10^4 Å. Thus, in consideration of the experimental results of drying as mentioned later, B1 and B6 bricks, respectively, have been taken for the typical specimen of comparatively smaller and larger pores. The liquids contained in the porous solids were water, *i*-butyl alcohol and glycerine solution arranged to various concentrations. The spherical shaped solids ($R = 25$ mm) contained with an appropriate amount of the said liquid (initial liquid content w_o) were to be hung in the dryer shown in Fig. 1.

† The sintered clay with pore size and porosity varied by burning carbon contained, after mixing kaoline powder with sieved coke powder (20–32, 60–65 and 100–200 mesh). These specimen, respectively, were referred to as specimens C20, C60 and C100.

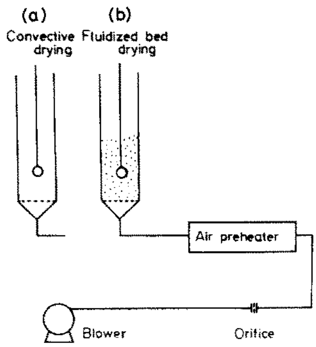

FIG. 1. Equipment.

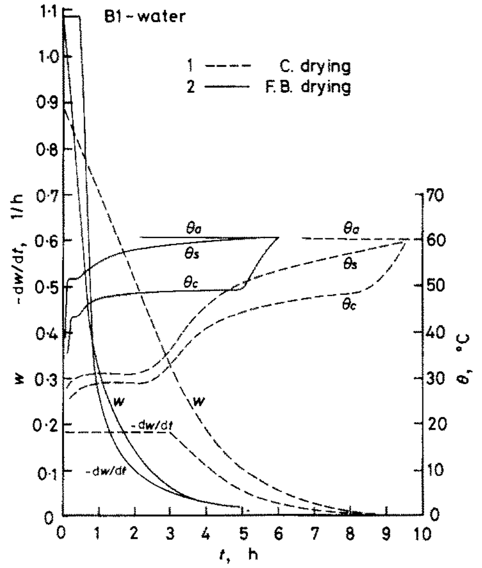

FIG. 2. Experimental results (B1–water).

Equipment

The experimental equipment is outlined in Fig. 1. It consists of three component parts; blower, air preheater and dryer. The dryer is 155 mm in diameter, 850 mm in height and is attached with three sheets of stainless steel wire gauge of 150 mesh to column bottom. In the case of fluidized bed drying, silica sands (20–100 mesh) and glass beads (1–2 mm dia.) as fluidizing particles are put on the said wire gauges to form the fluidized bed with hot air sent from the bottom [see Fig. 1(b)]. In the case of convective drying with only hot air, the fluidizing particles are not used in the dryer [see Fig. 1(a)]. The temperature changes of the specimen were measured on the spherical surface (θ_s), at the center of sphere (θ_c) and at the midpoint of the spherical surface and center (θ_m) with 0·3 mm dia. chromel–alumel thermocouples. The specimen was optionally taken out of the dryer to be measured its weight changes.

EXPERIMENTAL RESULTS AND CONSIDERATION

B1–*water*

The experimental results of B1–water system in Fig. 2 show larger increase of constant drying rate R_{sf} and larger reduction of total period required for drying in fluidized bed drying than in convective drying. From these facts, it can be easily understood that heat-transfer coefficient h_F and mass-transfer coefficient k_{HF} in fluidized bed are much larger than those (h_C, k_{HC}) in only gas flow.

$$R_{sf} = k_H(H_s^* - H_a) = \frac{h}{L}(\theta_a - \theta_s). \qquad (1)$$

As for temperature changes, the stable temperature (wet-bulb temperature) θ_I during constant rate period in fluidized bed drying was found to be much higher than that in convective drying. When the ratios of h_F to h_C and k_{HF} to k_{HC} were calculated by equation (1), the former was found to be much larger than the latter. (However, as for linear gas velocity u, $u_F/u_C \doteqdot 1/5$ as shown in Table 2.) Thus, in the fluidized bed, heat-transfer resistance reduced more than mass-transfer resistance in comparison with the case of convective drying, and heat- and mass-transfer rates were unbalanced [4]. The stable temperature θ_{II} (pseudo-wet-bulb temperature [2] or asymptotic temperature [5]) during falling rate period was almost equal in both fluidized bed and convective dryings, though both transfer resistances of heat and mass on the outer surface of the solids were widely changed. The second stable temperature θ_{II} is considered to be fixed from the dynamic equilibrium relation between heat- and mass-transfer rates both inside and outside solids. Thus, in the case of B1–water system, θ_{II} seems to depend mainly upon the transfer rates inside the solids.

B6—*water*

Figure 3 shows an example of experimental results in the case of B6–water system. As supposed from the pore distribution, the surface of the specimen B6 brick is rather rough, and so, when the specimen of the large initial liquid content was dried in the fluidized bed, the fluidizing particles were caught onto the surface of the specimen. (The surface of the specimen B1 brick is so smooth as not to catch the particles.) Therefore, the particles caught on the solid surface were involved in the weight of the specimen to be measured, and so, in the beginning, the apparent weight of the specimen increased. The "○" marked in Fig. 3 is the water content involving the particles caught on the solid surface. In order to find the net loss of water, the following measurement was performed.

Table 2. Experimental conditions

Fig.	System	Line or mark	Method	θ_a [°C]	W_s [g]	W_o [g]	w_o	u [cm/s]	Fluidizing particle
2	B1–water	1	C	60·0	47·3	42·2	0·892	110·0	
		2	F	60·5	43·1	48·7	1·130	21·5	Sand below 60 mesh
3	B6–water	1	C	60·0	59·9	39·4	0·658	110·0	
		2	F	69·0	58·8	38·6	0·656	31·1	Sand below 60 mesh
4	B6–water	⌀			52·1	36·3	0·697		
		○			53·0	37·0	0·698		
		△	F	61·0	56·1	39·4	0·702	30·4	Sand below 60 mesh
		●			59·3	38·8	0·654		
		×			57·5	42·5	0·739		
5	B6–water		F	100	54·6	36·6	0·671	68·4	Sand 20–30 mesh
6	B6–water		F	100	52·3	7·74	0·148	68·4	Sand 20–30 mesh
7	B6–glycerine	1		150	59·1	43·6	0·737	47·4	
		2	F	200	59·3	43·5	0·734	51·0	Sand 30–40 mesh
		3		300	59·4	43·4	0·731	63·5	
8	B6–glycerine solution†					‡	§		
	0%	1			60·1	33·4/33·4	0·556		
	10%	2			59·0	33·3/30·0	0·509		
	30%	3	F	150	58·4	37·9/26·5	0·454	47·4	Sand 30–40 mesh
	50%	4			58·8	37·4/18·7	0·318		
	100%	5			59·1	43·6/0	0		

Method C: convective drying.
Method F: fluidized bed drying.
† Glycerine concentration (weight %).
‡ A/B A: weight of contained glycerine solution; A/B B: weight of contained water.
§ Water content: B/W_s.

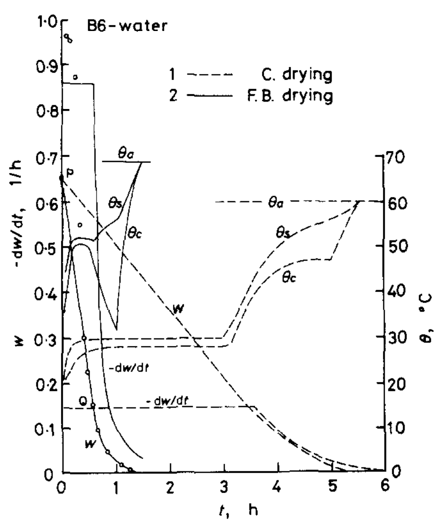

FIG. 3. Experimental results (B6–water).

Five pieces of specimen B6 brick containing the initial water content W_o were hung inside fluidized bed to dry for a given time, and after then, they being taken out, each of the following values was measured (see Fig. 4).

Diameter of specimen catching particles on its surface $= D'$ (2)

$$\text{Total weight } W_T = W_s + W_1 + W_p + W_2 \tag{3}$$

After the particles were removed from the specimen,

$$\text{Weight of wet specimen} = W_s + W_1 \tag{4}$$

$$\text{Weight of wet particles} = W_p + W_2 \tag{5}$$

then, after drying the wet specimen and particles,

$$\text{Weight of dry specimen} = W_s \tag{6}$$

$$\text{Weight of dry particles} = W_p. \tag{7}$$

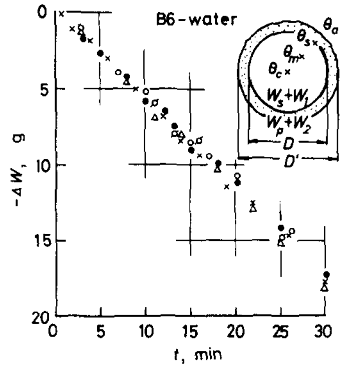

FIG. 4. Variation of net loss of water in fluidized bed dryer.

After then, the specimen was contained with the initial water content W_o to be hung inside the bed again. Net loss of water ($-\Delta W$) was calculated by the following equation and illustrated with time, the figure appears in almost a straight line (Fig. 4):

$$\text{net lost water} = -\Delta W = W_0 - W_1 - W_2 . \quad (8)$$

According to the above-mentioned, in the case of the specimen B6 brick also, the constant drying rate R_{sf} was considered apparently to exist, in spite that the particles were caught on the solid surface. In this case, the apparent spherical diameter D' reached maximum of 53–55 mm in 5–10 min after the specimen was hung in the fluidized bed, and then, these particles started to come off in turn from the lower portion to the upper portion of the specimen. After 30 min, no particle was found on the solid surface, and at the same time, the net loss of water began to be off from the straight line in Fig. 4. It was considered to come into the falling rate period. Thus, in the initial period, the net loss of water changed rectilinearly regardless to the amount of the particles caught on the solid surface. Therefore, in Fig. 3, connecting straightly between measured points P and Q of water content w, the drying rate $-\mathrm{d}w/\mathrm{d}t$ was calculated.

On the other hand, the temperature distribution in B6–water system showed abnormal temperature flucutation in the fluidized bed drying, though it clearly showed the first and second stable temperature in the convective drying (see Fig. 3). It was confirmed that such abnormality should be fully reproducible under the same fluidization condition.

Effect of fluidizing particles

The abnormal temperature fluctuation in B6–water system should appear in various ways under the different fluidization conditions. In a case of glass beads (1–2 mm dia.) used as the fluidizing particle, the abnormal fluctuation occurred, but the shape was not the same as in a case of fine silica sand particles. The glass beads used herein were considered to be large enough in diameter for the surface roughness of B6 brick, because very few particles were caught on the surface.

Effect of initial water content

Figures 5 and 6 show the effect of the initial water content w_o on the abnormality in fluidized bed drying of B6 brick. As the silica sands of 20–30 mesh were used as the fluidizing particles, the particles were found to be caught on the solid surface in the case that w_o was rather large (Fig. 5), but no particle was found when the drying started with the low water content (Fig. 6). In the case of high water content, two temperature peaks were observed, but in the case of low water content, only one peak corresponding to the second peak was observed. From these phenomena, it was found that the abnormality in the temperature change of B6 brick was not caused by the fluidizing particles caught on the solid surface.

In addition, the higher the heating temperature became, the more remarkable the abnormality was. And also, in the case of 37·5°C on the low temperature range, this phenomenon was clearly observed.

Effect of pore sizes

To examine the effect of pore sizes of solids on the abnormality, experiments of sintered clay–water system were carried out. The sintered clay were produced by burning out the mixtures of the clay powder and sieved coke powders. The pores were confirmed by microscopic observation to be almost same in size as the mixed carbon particles, and so the specimens were classified with the sizes of the contained coke powders. At $\theta_a = 150$°C, C20 and C60 had an only temperature peak, respectively. C100 had two peaks, and it could be considered that there existed the period corresponding to the constant rate period, though it was short. The larger the pore diameter of the specimen became, the more remarkable the abnormality was.

Effect of contained liquids

In B6–butyl alcohol (B.P. 108°C) system, the abnormality in the temperature change was observed in fluidized bed drying as well as in B6–water system.

Figure 7 shows the experimental results of B6–glycerine system (B.P. 290°C). At $\theta_a = 150$°C, the heating temperature was much lower than the boiling point and the evaporation was very slow. Thus, it showed the progress of temperature just like the case of unsteady heating. At $\theta_a = 200$°C, the evaporation became a little active, and the phenomenon of dropping the center temperature was slightly observed. And at $\theta_a = 300$°C, the said abnormality was distinctly observed as well as in the cases of B6–water and -*i*-butyl alcohol systems.

Figure 8 shows the experimental results of B6–

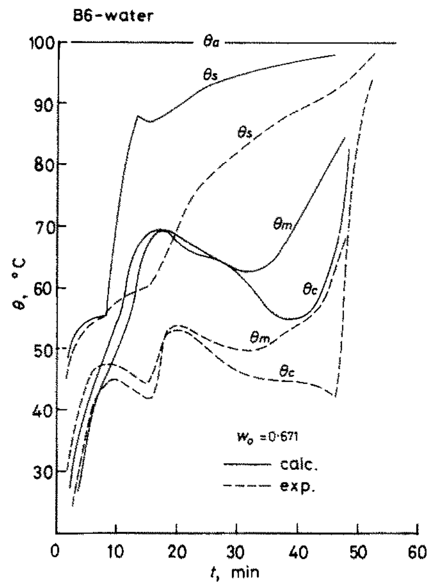

FIG. 5. Comparison of experimental results with numerically calculated results (B6–water, $w_o = 0{\cdot}671$, $h = 180$, $k_H = 140$, $k_v = 110$).

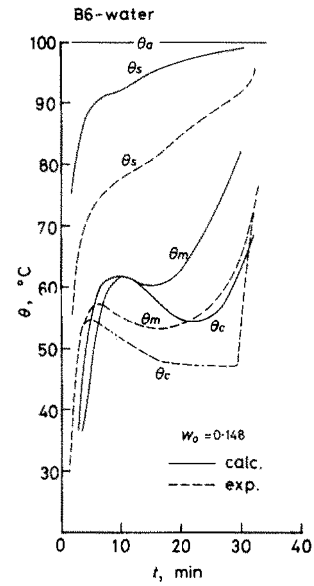

FIG. 6. Comparison of experimental results with numerically calculated results (B6–water, $w_o = 0{\cdot}148$, $h = 180$, $k_H = 140$, $k_v = 110$).

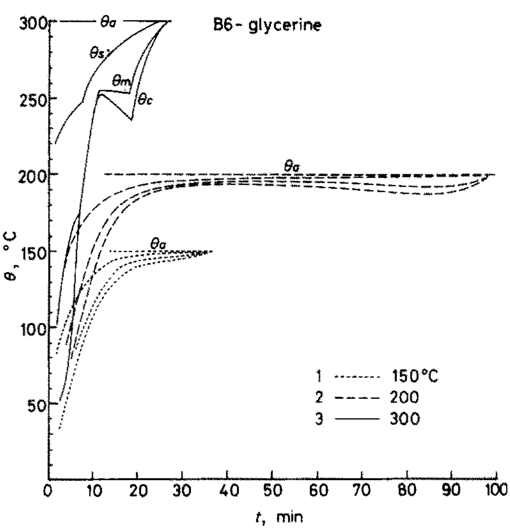

FIG. 7. Effects of heating temperature (B6–glycerine).

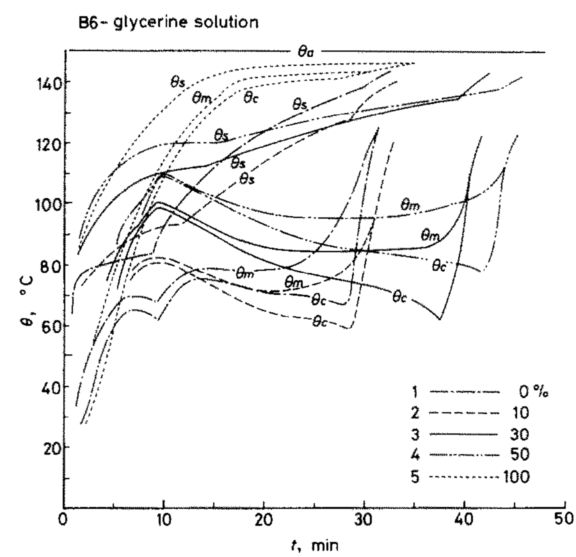

FIG. 8. Experimental results (B6–glycerine solution).

glycerine solution system ($\theta_a = 150$°C) in order to examine the effect of liquid properties (viscosity, surface tension etc.). Except the case of pure glycerine used, the abnormality of temperature change was generally observed, though the liquid properties were widely varied. Curve 2 for 10 per cent glycerine solution was similar to curve 1 for water, except that the former had an only peak but the later had two peaks. As the glycerine content increased, inner temperature of solids increased because glycerine prevented the internal evaporation and the liquid transfer of water.

On the other hand, as for B1 brick, the abnormality was not observed in the case of any other liquids as well as water.

COMPARISON OF CALCULATED RESULTS WITH EXPERIMENTAL ONES

From the above mentioned experimental results, it was found that, the larger the pore diameter of the specimen became, the more remarkable the abnormality of the temperature change was. Especially, in drying the specimen B6 bricks containing the various liquids, the said abnormality was widely observed. As the drying rate should be determined simultaneously with four rates of heat, liquid, vapor transfer and local evaporation, naturally the abnormality was considered as the phenomenon caused by mutual reaction among these four rates, but it was not clear which of the four gave the largest effect. In the previously presented paper [1], the authors reported the numerical calculation method of the drying rate, which can be applied synthetically to the whole drying period from high to low water contents by collective consideration of these four rates, and showed that the theoretical calculations agreed fairly well with the experimental data in the case of convective drying. And then, the numerical method should be considered very effective in the analysis of abnormality in the present paper (the numerical method is shown in Appendix).

Figures 5 and 6 show the comparison between theoretical and experimental values. Figure 5 shows the comparison of the experiments started from the high initial water content ($w_o = 0{\cdot}671$). As mentioned above, as for the specimen B6 brick, the fluidizing particles were caught on the solid surface with this initial water content. The state of the particles caught on the solid surface was too much complicated, and so the effects of the particles on heat- and mass-transfer rates were not taken into consideration in the case of theoretical calculation. Accordingly, in the theoretical calculation, the first stage period was too short in comparison with the experimental results. On the contrary, the tendency of temperature drop inside the solid during the second stage period (corresponding to the falling rate period) could be shown well by theoretical calculation, but the absolute value itself was a little different from the experimental value. Figure 6 shows the case with the low initial water content ($w_o = 0{\cdot}148$). In this case, no fluidizing particle was found to be caught on the solid surface, and also the falling rate period started from the beginning. The temperatures took a little higher values in theoretical calculation than in experiment. In Fig. 6, however, the phenomenon of temperature drop was well explained by the theory. Thus, the theoretically analysing method in the previous paper could be very available for the conditions under which the said surface resistances was to be remarkably reduced, that is to say, which both heat- and mass-transfer rates on the surface was so large.

SUMMARY

The wet porous solids were dried inside the fluidized bed, availing the fact that heat- and mass-transfer coefficients between fluidized bed and solid placed herein, are remarkably larger than ones in the forced convection by only air flow. As the result, as for the specimen of comparatively small pore diameter such as B1 brick, the experimental results were similar to ones to be expected from the conventional drying theory, and on the contrary, as for the specimen B6 brick of larger pore diameter, the abnormality that the internal temperature goes on dropping in process of drying was found. In the usual convective drying and radiation drying of either specimen, no abnormality was found. It seemed that occurrence of such an abnormality depended on the ratio of both heat- and mass-transfer resistances of the specimen's surface and interior. It was presumed that, the smaller was the diffusion resistance of vapor produced inside the solid, the more remarkably the abnormality was observed. Then, on the basis of the theoretical calculation applied with a synthetically analysing method of the whole drying period, the abnormality in temperature change could be explained fairly well. The drying of porous solids synthetically depends upon four rates of heat, liquid and vapor transfer and local evaporation, and accordingly the abnormality of temperature change in the case of fluidized bed drying seems to be affected by many factors. It was regarded that this analytical method was available for explanation of the abnormal phenomenon.

Acknowledgement—The theoretical calculations in this paper were performed with the computer FACOM 230-60 of Nagoya University Computation center.

REFERENCES

1. M. Nakamura and S. Sugiyama, A consideration on the drying rate of porous solids, *Kagaku Kogaku* (*Chem. Engng, Japan*) **35**, 1122–1125 (1971); *Heat Transfer—Japanese Research* **1**(2), 89–92 (1972).
2. A. H. Nissan, W. G. Kaye and J. R. Bell, Mechanism of drying thick porous bodies during the falling rate period I. The pseudo-wet-bulb temperature, *A.I.Ch.E. Jl* **5**, 103–110 (1959).
3. M. Shimizu, F. Watanabe and S. Sugiyama, Effective diffusion coefficient of gas in porous materials and granular beds, *J. Chem. Engng Japan* **4**, 331–336 (1971).
4. T. Shirai *et al.*, Heat and mass transfer on the surface of solid spheres fixed within fluidized beds, *Kagaku Kogaku* (*Chem. Engng, Japan*) **29**, 880–884 (1965).
5. R. Toei *et al.*, The mechanism of drying of a bed of granular and powdered materials during the second falling rate period, *Kagaku Kogaku* (*Chem. Engng, Japan*) **28**, 458–467 (1964).
6. E. N. Ziegler and W. T. Brazelton, Mechanism of heat transfer to a fixed surface in a fluidized bed, *I/EC Fundamentals* **3**, 94–98 (1964).

APPENDIX

Basic Equations

The authors have presented previously the analytical method of the drying rate of porous solids synthetically through the whole process from high water content to low one. This method could be summarized as follows:

As for the unsteady heat-conduction equation accompanied with evaporation:

$$C_e\rho_e \frac{\partial\theta}{\partial t} = \frac{1}{r^2}\frac{\partial}{\partial r}\left(\lambda_e r^2 \frac{\partial\theta}{\partial r}\right) - LR_{\text{loc}}. \quad \text{(A1)}$$

As for the water transfer inside the solid;

$$\frac{\partial w}{\partial t} = \frac{1}{r^2}\frac{\partial}{\partial r}\left(D_w r_2^2 \frac{\partial w}{\partial r}\right) - \frac{R_{\text{loc}}}{\rho_o}. \quad \text{(A2)}$$

As for the vapor transfer;

$$\frac{\partial v}{\partial t} = \frac{1}{r^2}\frac{\partial}{\partial r}\left(D_v r^2 \frac{\partial v}{\partial r}\right) + \frac{R_{\text{loc}}}{\rho_o}. \quad \text{(A3)}$$

And as for the local evaporation rate;

$$\frac{R_{\text{loc}}}{\rho_o} = k_{\text{evap}}\, a_i(v^* - v). \quad \text{(A4)}$$

Each of these equations can be considered to hold. The driving force for the water transfer inside porous solid has been regarded as a so-called suction potential, but in this paper, we adopted an expedient based on the water content gradient. w and v represent water content and vapor content inside the solid, respectively. k_{evap} is mass-transfer coefficient (local evaporation rate coefficient) between liquid and vapor phases inside solid, and a_i is the effective interfacial area for local evaporation inside the solid. The mark "*" means the saturated value.

Initial and Boundary Conditions

$$t = 0,\quad 0 \leqslant r \leqslant R;\qquad \theta = \theta_o,\quad w = w_o,\quad v = v_o \quad \text{(A5)}$$

$$t > 0,\quad r = 0;\qquad \frac{\partial\theta}{\partial r} = \frac{\partial w}{\partial r} = \frac{\partial v}{\partial r} = 0 \quad \text{(A6)}$$

$$t > 0,\quad r = R;\qquad \lambda_e \frac{\partial\theta}{\partial r} = h(\theta_a - \theta_s) + a_s k_H (H_a - H_s^*)L \quad \text{(A7)}$$

$$\rho_o D_w \frac{\partial w}{\partial r} = a_s k_H (H_a - H_s^*) \quad \text{(A8)}$$

$$D_v \frac{\partial v}{\partial r} = (1 - a_s) k_v (v_a - v_s). \quad \text{(A9)}$$

Various Parameters

Various parameters shown in equations (A1)–(A9)—C_e, ρ_e, λ_e, D_w, D_v, a_i and a_s—vary largely their values in drying process, and so in the previous paper [1], the influence of water content w on each parameter was taken into the consideration in theoretical calculation. In this paper, the same consideration was taken, except D_v was conformed to the following equation:

$$D_v = \frac{P}{P - p}\frac{\varepsilon_e D_{vo}}{\eta^2} \quad \text{(A10)}$$

where, P means total pressure, ε_e porosity and η tortuosity factor.

Numerical Analysis

The variations of temperature θ and water content w in the porous solid in drying process shall be obtained by simultaneously solving the fundamental differential equations (A1)–(A3) and local evaporation rate equation (A4) under the conditions of (A5)–(A9), but equations (A1)–(A3) are non-linear. Therefore, in order to solve them analytically, it is required to provide many assumptions. In such case, in the consideration that numerical analysis to lessen assumptions is more practical than analytical solution, the numerical calculations have been made by developing the fundamental equations into difference equations on time t and distance r.

EFFETS DES RESISTANCES DE SURFACE SUR LES TRANSFERTS SIMULTANES DE CHALEUR ET DE MASSE DANS LES SOLIDES POREUX AVEC CHANGEMENT DE PHASE

Résumé—Le mécanisme du séchage et la vitesse de séchage des solides poreux dans les dessicateurs à air chaud ont été largement analysés et systématisés par voie théorique. Néanmoins lorsque les solides humides sont séchés dans un lit fluidisé en utilisant le fait de coefficients de transfert remarquablement élevés entre le lit et le solide, on constate le phénomène d'une température interne qui diminue pendant le séchage. Cette circonstance inhabituelle n'a jamais été prévue par les théories conventionnelles. Dans cet article, les auteurs sèchent dans un lit fluidisé différentes sphères solides humides et essaient d'analyser ce phénomène en utilisant une méthode analytique du séchage, présentée antérieurement par eux.

EINFLUß DES OBERFLÄCHENWIDERSTANDS AUF GLEICHZEITIGE WÄRME UND STOFFÜBERTRAGUNG MIT PHASENWECHSEL IN PORÖSEN FESTKÖRPERN

Zusammenfassung—Der Trockenmechanismus und der Trocknungsgrad von porösen Festkörpern in üblichen Heißlufttrocknern wurden ausgiebig untersucht und theoretisch systematisiert. Immer dann, wenn feuchte Festkörper in einer Wirbelschicht getrocknet wurden—in Anwendung der Tatsache, daß die Wärmeübergangskoeffizienten zwischen Wirbelschicht und Festkörpern bemerkenswert groß sind—

wurden so ungewöhnliche Erscheinungen gefunden wie ein Innentemperaturabfall während des Trockenvorgangs. Derartige unübliche Vorgänge wurden bisher von den konventionellen Theorien für Heißlufttrockner nicht berücksichtigt.

Bei den Untersuchungen zu diesem Bericht trockneten die Autoren in einer Wirbelschicht verschiedene Feststoffmengen, die Flüssigkeiten enthielten und versuchten so, unter Anwendung der analytischen Methode zur Bestimmung des Trocknungsgrades, ungewöhnliche Erscheinungen zu analysieren.

ВЛИЯНИЕ ПОВЕРХНОСТНЫХ СОПРОТИВЛЕНИЙ НА ОДНОВРЕМЕННЫЙ ТЕПЛО- И МАССООБМЕН В ПОРИСТЫХ ТВЕРДЫХ ТЕЛАХ ПРИ НАЛИЧИИ ФАЗОВЫХ ПЕРЕХОДОВ

Аннотация — К настоящему времени широко изучены и теоретически систематизированы механизм и скорость сушки пористых твердых тел в обычных сушилках с горячим воздухом. Однако, в период сушки влажных твердых тел в кипящем слое при довольно больших коэффициентах теплообмена обнаружено такое необычное явление как падение внутренней температуры по мере высыхания. Это явление не вытекает из обычных теорий сушилок с горячим воздухом.

Авторы данной работы изучали процесс сушки различных твердых сфер, содержащих жидкость, в кипящем слое и пытались проанализировать это необычное явление с помощью аналитического метода сушки, который был ранее представлен ими.